AGU ADVANCING EARTH AND SPACE SCIENCES

Geophysical Research Letters

RESEARCH LETTER
10.1029/2025GL117846

Resolution and Frequency-Dependent Climate Signals in an Arctic Tree-Ring Temperature Reconstruction of the Last Millennium

Julie Edwards[1,2,3], Kevin J. Anchukaitis[2,3,4], Francisca Molina[2], Laia Andreu-Hayles[4,5,6], Rosanne D'Arrigo[4], and Georg von Arx[7,8]

[1]Bren School of Environmental Science & Management, UC Santa Barbara, Santa Barbara, CA, USA, [2]School of Geography, Development, and Environment, University of Arizona, Tucson, AZ, USA, [3]Laboratory of Tree-Ring Research, University of Arizona, Tucson, AZ, USA, [4]Lamont-Doherty Earth Observatory of Columbia University, Palisades, NY, USA, [5]Centre for Ecological Research and Forestry Applications (CREAF), Barcelona, Spain, [6]Catalan Institution for Research and Advanced Studies (ICREA), Barcelona, Spain, [7]Swiss Federal Institute for Forest Snow and Landscape Research WSL, Birmensdorf, Switzerland, [8]Oeschger Centre for Climate Change Research, University of Bern, Bern, Switzerland

Key Points:

- Tree-ring density measurement resolution affects low-frequency trends in temperature reconstructions
- High-resolution anatomical maximum latewood density has stronger correlations with instrumental temperature across frequencies
- New temperature reconstruction from high-resolution density measurements shows colder pre-industrial climate than previous reconstructions

Supporting Information:

Supporting Information may be found in the online version of this article.

Correspondence to:

J. Edwards,
j_edwards@ucsb.edu

Citation:

Edwards, J., Anchukaitis, K. J., Molina, F., Andreu-Hayles, L., D'Arrigo, R., & von Arx, G. (2025). Resolution and frequency-dependent climate signals in an Arctic tree-ring temperature reconstruction of the last millennium. *Geophysical Research Letters*, *52*, e2025GL117846. https://doi.org/10.1029/2025GL117846

Received 30 JUN 2025
Accepted 9 OCT 2025

Abstract Paleoclimatology makes it possible to place recent climate changes in a longer-term context than is available from the instrumental record. Tree-ring reconstructions, often used to quantify temperature variations over the Common Era, contain multiple uncertainties that affect estimates of the magnitude of recent trends and past variability. The use of maximum latewood density (MXD) proxy mitigates many biases, but intra-annual measurement resolution remains a limitation. We develop a quantitative wood anatomy (QWA)-based temperature reconstruction from the Firth River in northeastern Alaska from 1150 CE to 2021 CE to improve regional past temperature estimates and to test the sensitivity of MXD-based climate reconstructions to measurement constraints. We find that high-resolution wood-anatomy measurements reduce biological noise and enhance the representation of low-frequency variability, resulting in stronger temperature signals and a larger magnitude of preindustrial to modern change. QWA data provide novel high-resolution information that improves tree-ring temperature reconstructions.

Plain Language Summary This study investigates the effect of tree-ring measurement resolution on temperature reconstructions using millions of individual cellular dimensions from white spruce trees at the Arctic treeline. Although the maximum latewood density tree-ring measurement (MXD) has been shown to capture temperature variability, uncertainties remain due to varying measurement resolutions. By using high-resolution quantitative wood anatomical data, especially anatomical MXD (aMXD), this research aims to refine the skill of climate reconstructions. The use of high-resolution aMXD can mitigate biases found in traditional MXD, which is often at a lower measurement resolution. High-resolution aMXD shows stronger correlations with instrumental temperature records at both high-and low-frequency, indicating its enhanced reliability for reconstructing past climates over long periods of time and capturing recent temperature trends. These results demonstrate the benefits of using high-resolution wood anatomy data to reconstruct past temperature. Applying this method to other regions can enhance our understanding of climate variability and trends across space and time.

1. Introduction

Understanding long-term temperature fluctuations and their magnitudes relative to the modern warming trend is crucial for better projections of future climate change (Tierney et al., 2020). Paleoclimate reconstructions of the past millennium provide an extended high-resolution (seasonal to annual) perspective on Earth's climate variability and trajectory, which is not available from the relatively short instrumental record (Christiansen & Ljungqvist, 2017; Mann & Jones, 2003). Tree-ring data in particular are often used to characterize late Holocene temperature variations and are the major proxy used in the Common Era reconstructions assessed in the IPCC reports (Anchukaitis & Smerdon, 2022; Masson-Delmotte et al., 2021). Ongoing debates about Common Era climate reconstructions have focused on the ability of the two most commonly used proxy observations, tree-ring width and maximum latewood density (MXD), to accurately and precisely reflect climate change over this time span (Briffa et al., 1996; Büntgen, 2022; Esper et al., 2012, 2015, 2016), to capture the full amplitude of climate

extremes (Battipaglia et al., 2010; McCarroll et al., 2015), and to express the full frequency range of climate variability (Franke et al., 2013; Lücke et al., 2019).

Ensemble-based approaches (Büntgen et al., 2021; PAGES 2k Consortium, 2019), attempt to address uncertainties arising from weakly constrained statistical and methodological choices. Nevertheless, there remain several sources of uncertainty and bias in tree-ring data that affect the interpretation of individual and large-scale temperature reconstructions. Of particular concern is the capture of low-frequency climate variability (Esper et al., 2004, 2012; Lücke et al., 2021). Non-climatic age-related trends in tree-ring data typically require detrending, which can limit the frequencies captured in tree-ring reconstruction but also impart its own biases (Briffa & Melvin, 2011; Cook et al., 1995). Finally, tree-ring width, the most widely used tree-ring measurement, is known to have very weak and temporally unstable correlations with temperature in high-latitude northwestern North America (Andreu-Hayles et al., 2011; Briffa et al., 2002), which limits its use in temperature reconstructions of this region.

The use of MXD in temperature reconstructions has mitigated many of these uncertainties and biases (Björklund et al., 2019; Esper et al., 2015; Schneider et al., 2015). A remaining issue with traditional MXD is measurement resolution, which is not standardized across methods or between institutions (Björklund et al., 2019). One alternative to traditional MXD is blue intensity, which uses light reflectance to estimate wood density (Campbell et al., 2007; McCarroll et al., 2002; Rydval et al., 2014), but can be biased by discoloration and low image resolution (Rydval et al., 2024). Björklund et al. (2019) found that a decline in ring width results in a proportional decline in MXD values when the measurement resolution of the latter is low, which therefore affects the capacity of MXD to accurately represent long-term trends. Quantitative wood anatomy (QWA) approaches to developing MXD proxy data can provide much higher resolution intra-annual measurements, resolving cellular scale characteristics of the annual ring (Von Arx et al., 2016). QWA temperature reconstructions have recently revised the Common Era temperature history of Scandinavia, showing a better match with climate models, particularly during the Medieval Climate Anomaly (MCA) (Björklund et al., 2023).

Here, we develop new QWA tree-ring data from the Firth River in northeastern Alaska (Anchukaitis et al., 2013; Andreu-Hayles et al., 2011), which is an important site as there are still relatively few long tree-ring records in this region. The existing Firth River series is used in many large-scale Northern Hemisphere temperature reconstructions (Anchukaitis et al., 2017; Schneider et al., 2015; Stoffel et al., 2015; Wilson et al., 2016). QWA has several potential advantages over both annual ring width and traditional MXD: first, extremely high-resolution measurements of individual tracheid cell dimensions should improve temperature reconstruction at both high and low frequencies (Björklund et al., 2019). Second, by using QWA data we can evaluate how the resolution of wood density measurements affects the sensitivity of tree-ring data to temperature variability. Finally, cell anatomical dimensions have a well-understood biological and functional foundation, permitting an understanding of the mechanistic link between climate and growth response (Björklund et al., 2020; Edwards et al., 2025; Hacke et al., 2001; Seftigen et al., 2022). The objective of our study is to leverage the strengths of QWA data to improve Arctic temperature reconstructions and to test the sensitivity of MXD-based climate reconstructions to constraints due to measurement resolution. Our study demonstrates the value of developing QWA chronologies for climate reconstruction and provides new information about the temperature history of northwestern North America, one of the most rapidly warming regions in the world (Masson-Delmotte et al., 2021).

2. Data and Methods

Living and subfossil wood samples of white spruce (Picea glauca) were collected from the Firth River near Mancha Creek at latitudinal treeline (68.67°N, 141.05°W) in summer of 2022. These samples were used to extend and augment an existing collection from the same location (Anchukaitis et al., 2013). Ring-width measurement and cross-dating for the combined collection was developed following standard dendrochronological procedures (D'Arrigo et al., 2014; Stokes & Smiley, 1968). We selected 57 trees for additional QWA analysis, prioritizing a consistent sample depth, a range of age classes, and correlation with the overall ring-width chronology ($r > 0.4$). These samples span from 1069 to 2021 CE (952 years) with a mean segment length of 219 years (range from 107 to 384 years).

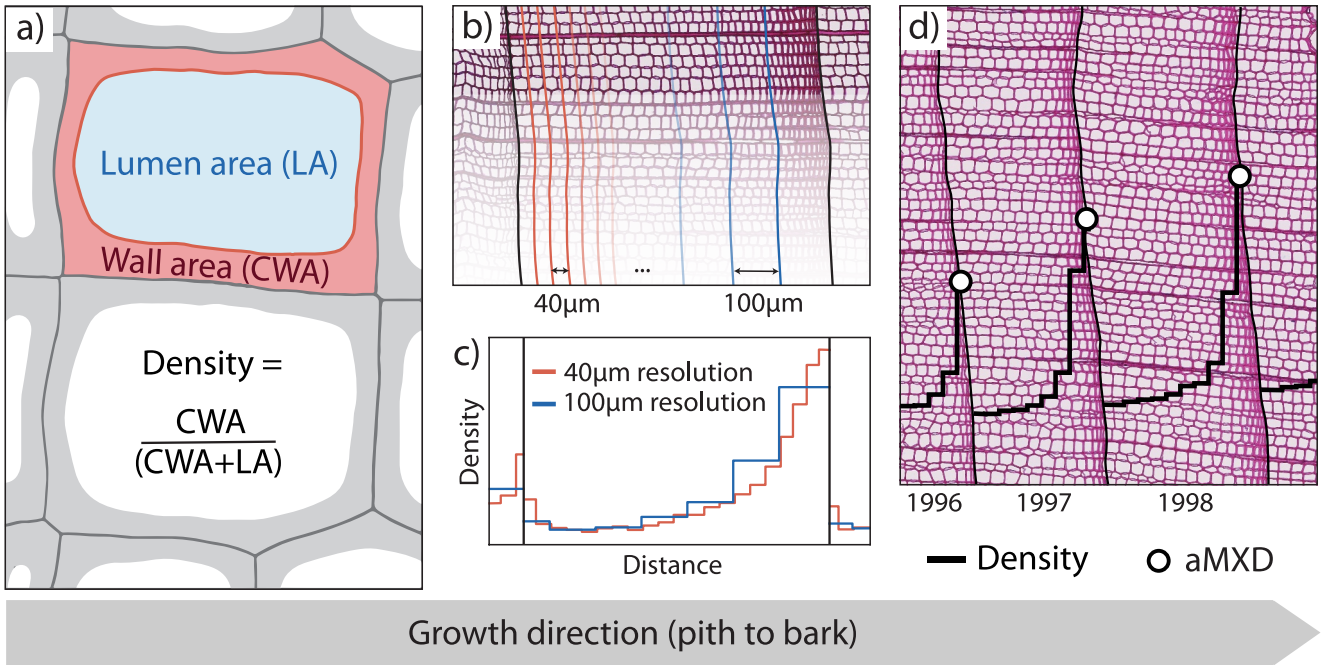

Figure 1. Conceptual diagram of how anatomical maximum latewood density (aMXD) is measured. Illustration of the cell dimensions used to calculate the anatomical density for each cell in this study: cell-wall area, lumen area (LA) (a). Cell measurements are aggregated at intra-annual bands of 40 µm (red) and 100 µm (blue), which determine the resolution of the final measurements (b). Intra-annual profiles of density resulting from the 40 µm (red) and 100 µm (blue) band widths (c). Maximum values of density were extracted from the intra-annual profiles to return the anatomical MXD for each resolution, measurements for the 40 µm are shown (d).

2.1. Quantitative Wood Anatomy

We cut the wood samples to a thickness of 10–12 µm using a rotary microtome (Microm HM355S). The microsections were stained with a 1% safranin solution, permanently fixed in Eukitt, and prepared following standard procedures (Fonti et al., 2025; Gärtner & Schweingruber, 2013; von Arx et al., 2016). Digital images of the microsections were produced at the Swiss Federal Research Institute WSL in Birmensdorf, Switzerland, using a Zeiss Axio Scan Z1. The ROXAS (v3.1) image analysis software (Prendin et al., 2017; von Arx & Carrer, 2014) was used to measure tracheid cell characteristics after automatic detection from microsection images using a deep-learning model (Katzenmaier et al., 2023). We excluded measurements of cells with cell walls damaged during sampling or preparation. In total, approximately 14,850,000 cells were measured at an image resolution of 0.44 µm per pixel (57,727 dpi).

Lumen area and cell-wall area were measured for every cell and then used to calculate density as the ratio between lumen area and the total cell area (Figure 1a) (Björklund et al., 2020). Within each annual ring, individual cellular measurements were aggregated within equal-size bands of 10, 20, 40, 80, and 100 µm width to test the effect of measurement resolution (Figure 1b). Within each band, the cell measurements were aggregated using two methods, a biweight mean (Cook et al., 1990) and the 75th percentile value (Q75; Björklund et al., 2020) to test the effect of the aggregation method. The importance of this particular choice for QWA climate reconstructions has not yet been investigated. For each resolution and aggregation method, the maximum value calculated within each ring is the anatomical MXD (aMXD) for that year (Figure 1d). Although cell wall thickness alone has been shown to slightly outperform aMXD for temperature reconstruction (Björklund et al., 2023; Lopez-Saez et al., 2023; Seftigen et al., 2022), we use aMXD here due to its closer relation to traditional MXD. Latewood widths were determined by Mork's index at a 10 µm resolution (Denne, 1989; Mork, 1928).

2.2. Chronology Development

We created multiple aMXD chronologies to test the sensitivity of chronology statistics to four varying parameters (Text S1 in Supporting Information S1). These include: (a) the intra-annual band width (as described above and referred to as the "resolution" henceforth), (b) the measurement aggregation method, (c) the application of a

power transformation to the data prior to detrending (Cook & Peters, 1997), and (d) the detrending method: either Regional Curve Standardization (RCS; Briffa & Melvin, 2011) or Signal-Free RCS (Homfeld et al., 2024; Melvin & Briffa, 2008) using the CRUST software (Melvin & Briffa, 2014a, 2014b). We used an age-dependent spline (Melvin et al., 2007) and included estimated pith-offsets for both RCS and Signal-Free RCS detrending.

For the final reconstruction, we use the aMXD chronology produced with the biweight mean aggregation method, power transformation, and Signal-Free RCS detrending. The power transformation was applied due to the negative Spread versus Level correlation (Cook & Peters, 1997) in the raw data. The Signal-Free RCS data was selected as Anchukaitis et al. (2013) previously found that Signal-Free RCS was the least biased of the detrending choices for Firth River MXD data based on simulated pseudoproxy MXD data. Biweight mean aggregation was used because it provides a representative average of all cells within an intra-annual band while still accounting for the influence of outliers. The 10 μm resolution (aMXD10) was used as the high-resolution example, consistent with the typical size of a latewood tracheid in the radial direction (Vaganov et al., 2006). The 20 μm resolution (aMXD20) was used as the next reasonable interval to test whether the 10 μm data might be overly fine and therefore introduce additional noise. Finally, the 80 μm resolution (aMXD80) was used as the low-resolution example, representative of the apparent resolution of a range of MXD collection methods (Björklund et al., 2019).

2.3. Climate Data Analysis and Reconstruction

We extracted daily ERA5 temperature data from the $0.5° \times 0.5°$ grid-cell over the Firth River site. The aMXD10 chronology was correlated against daily ERA5 using a moving mean starting at January 1st (Day-of-Year, DOY 1) and using a variable window size (from 1 to 91 days in width) from 1950 to 2021 CE. The window size and window center location with the highest correlation coefficient (see Section 3) was used as the temporal target for both the subsequent spatial correlation and as the reconstruction predictand (Jevšenak, 2019). We performed seasonal correlation analyses as described by Meko and Woodhouse (2011) to calculate the Pearson correlation between the aMXD10 chronology and monthly ERA5 temperature data using 1, 2, 3, and 4-month seasons from 1950 to 2021. We calculated the point-by-point Pearson correlation coefficient between the gridded ERA5 data of the 195–223 DOY mean temperature and the aMXD10 chronology. High-pass and low-pass butterworth filters were applied to the aMXD10, aMXD20, and aMXD80 chronologies, and correlated to ERA5 195–223 DOY mean temperature, which was filtered identically (Ols et al., 2023).

For the final reconstruction, we used the Composite Plus Scale (CPS; Jones & Mann, 2004) method with the aMXD chronology as the predictor and the ERA5 195–223 DOY mean temperature of the Firth River grid cell as the predictand. We used the full 1950–2021 CE period as the calibration period. The reconstruction start year was truncated to 1150 CE due to decreasing sample depth prior to that year (Figure S1 in Supporting Information S1). To assess reconstruction performance, we used a split calibration/validation period (early period: 1950–1985 CE; late period: 1986–2021 CE) and full period calibration/validation statistics $\left(R^2c, R^2v\right)$, coefficient of efficiency (CE), Reduction of Error (RE), and the Durbin Watson statistic (which tests for autocorrelation in the reconstruction residuals). We further analyze temporal stability using 21-year running correlations (1-year step) and apply the Gershunov test (Gershunov et al., 2001) to evaluate whether the observed correlation vary more than expected from chance and from the reduced effective sample size associated with the moving window.

We performed Superposed Epoch Analysis (SEA) to evaluate the response of the reconstructions to large volcanic eruptions. We used the eVolv2k_v3 data set (Toohey & Sigl, 2017) to create an event list of the top 20 eruptions between 1150 and 1900 CE, determined by Northern Hemisphere stratospheric aerosol optical depth. The event years are 1171, 1182, 1230, 1257, 1286, 1329, 1345, 1453, 1458, 1477, 1585, 1600, 1640, 1695, 1729, 1783, 1809, 1815, 1831, and 1883. Some of these eruption dates are not known precisely, which potentially introduces misalignment error in the SEA compositing. The aMXD response to volcanic eruptions is calculated by first removing the mean temperature of the 3 years prior to each event year (Year 0) and then averaging across all events. Uncertainty bounds at the 5th and 95th percentile were calculated based on a 1000 member Monte Carlo simulation drawing random event year lists for each reconstruction.

3. Results

Mean latewood width was 35.27 μm ± 25.17 μm. The parameter with the strongest impact on chronology statistics was the resolution, followed by the measurement aggregation method; the use of RCS or Signal-Free RCS

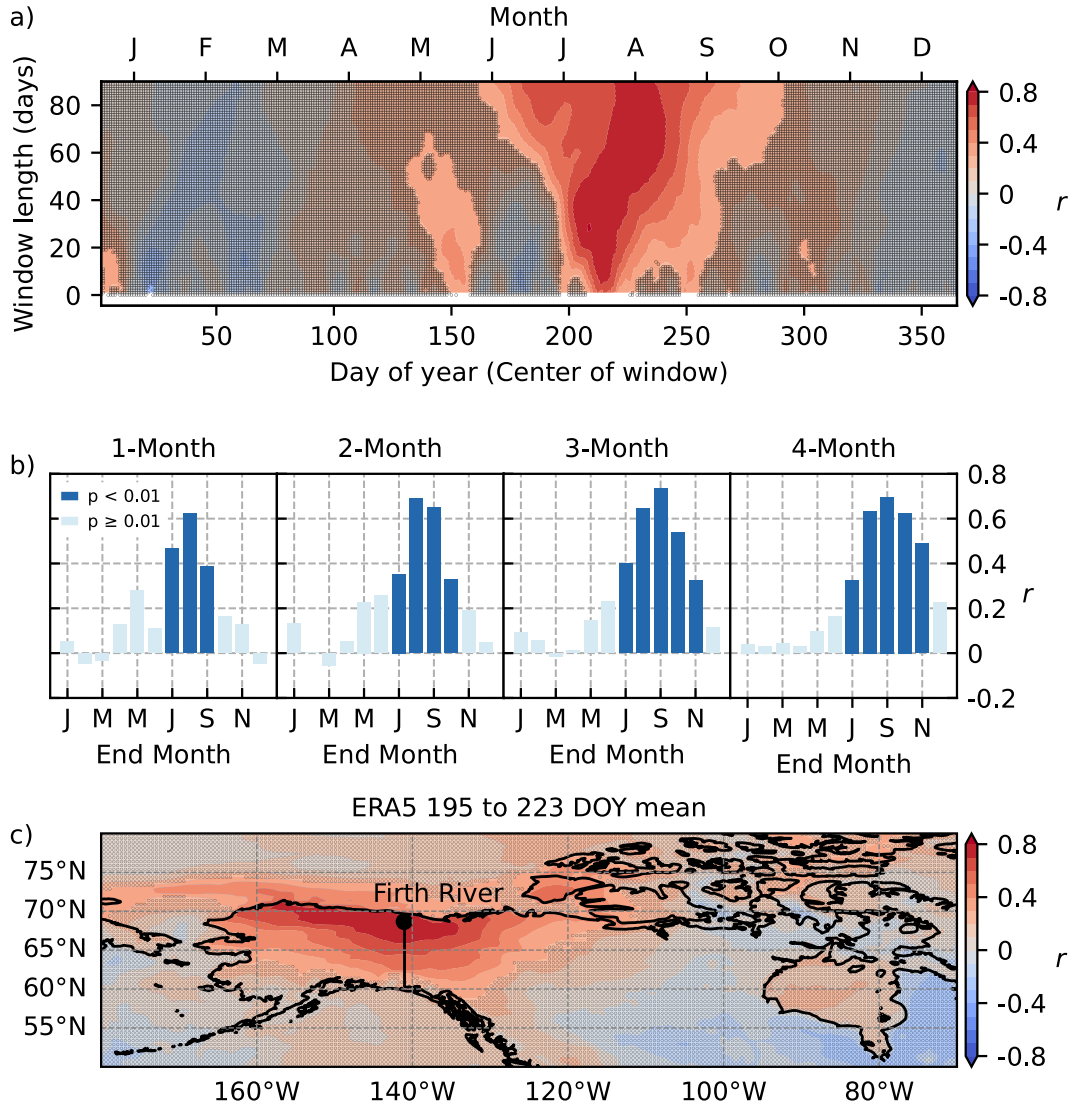

Figure 2. Correlations between ERA5 daily temperature and the aMXD10 chronology. The *x*-axis is the center of the moving mean window and the *y*-axis is the window length. Lack of stippling indicates significance ($p < 0.01$) (a). Seasonal correlations between monthly ERA5 data of the grid-cell over Firth River and the aMXD10 chronology at 1, 2, 3, and 4-month seasons. The End Month indicates the last month of a seasonal mean of the given length (b). Spatial correlation of the aMXD10 chronology with the ERA5 daily data averaged over the 195–223 DOY period. Lack of stippling indicates local significance ($p < 0.01$) (c).

detrending and the choice to power transform or not, had less of an impact (Text S1 and Figure S2 in Supporting Information S1).

The daily moving window correlations between temperature and aMXD10 show the strongest correlation ($r = 0.81$) at the 195–223 DOY window, which corresponds to approximately mid-July to mid-August (Figure 2a). The correlations are generally strong ($r \geq 0.7$) for varying windows over this entire time period, with weaker but significant positive correlations extending into early September. There is also a weaker but significant and positive correlation with mid-May to mid-June temperature. The strongest correlation in the seasonal analysis using monthly data is in the 3-month season ending in September ($r = 0.73$; Figure 2b). For the spatial correlation, the strongest correlation ($r \geq 0.7$) is centered on the Firth River site and extends longitudinally. There is a dipole pattern, with negative correlations in Eastern Canada, but this is not significant at the $\alpha = 0.01$ level (Figure 2c). Overall, correlations analyses across a range of temporal and spatial scales shows a significant and coherent late-summer signal.

The aMXD10 reconstruction of mid-July to mid-August (195–223 DOY) temperature early calibration (1950–1985 CE)/late validation (1986–2021 CE) yields $R_c^2 = 0.76$, $R_v^2 = 0.49$, RE = 0.32, CE = 0.31 and late calibration (1986–2021 CE)/early validation (1950–1985 CE) yields $R_c^2 = 0.49$, $R_v^2 = 0.76$, RE = 0.72, CE = 0.72, showing stable performance. The aMXD10 reconstruction of mid-July to mid-August temperature using the full period calibration performs well ($R^2 = 0.64$, RE and CE values of 0.60; pbw10, Table S1 in Supporting Information S1). The Durbin-Watson statistic is 1.99, indicating the reconstruction residuals do not have significant autocorrelation and therefore suggesting recent temperature trends are accurately reproduced. Moving correlation results (Figure S3 in Supporting Information S1) show that aMXD10 maintains a strong relationship with temperature. Although correlation coefficient values decline through the latter half of the record, reaching a minimum in the 1990s before recovering after 2000, the observed standard deviation values of the moving correlations fall within the range expected by chance and window length, as assessed by the Gershunov test (Gershunov et al., 2001).

The calibration/validation R^2 using a 72-year period (1950–2021 CE) decreases with lower resolution for the reconstructions (Figure 3a). The highest resolution aMXD10 reconstruction correlates strongly ($r \geq 0.7$) with ERA5 195–223 DOY mean temperature across frequencies (Figure 3b). The high-resolution aMXD20 correlates strongly ($r \geq 0.7$) across frequencies until the low-pass 20-year frequency. The low-resolution aMXD80 has smaller correlation coefficients across frequencies and there is a sharp decline in the correlation coefficient at the low-pass 20-year frequency. Correlations for frequencies beyond a 6-year low-pass filter are however not statistically significant ($p < 0.01$) when accounting for the resulting reduced degrees of freedom due to autocorrelation over this relatively short time period (Bretherton et al., 1999). Interestingly, the low-resolution reconstruction aMXD80 has more low-frequency variability and higher estimated temperatures in the pre-industrial period compared to the high-resolution reconstructions, aMXD10 and aMXD20 (Figure 3c), suggesting aliasing of the spectrum.

The SEA results show a significant temperature response to large volcanic eruptions at the event year (Figure 4). The aMXD80 chronology exhibits a significant response greater than −1°C in the year of the eruption, aMXD10 shows an approximately −1°C response, and the aMXD20 response is only barely significant. For the aMXD chronologies created with biweight aggregation, chronologies without the power transformation applied have a larger response than those with the power transformation (Figure S4a in Supporting Information S1). For the aMXD chronologies created with Q75 aggregation, those with the power transformation applied show a smaller response at the event year than the biweight chronologies. The Q75 chronologies without the power transformation show a significant response with a magnitude greater than −1°C (Figure S4b in Supporting Information S1). The 10 μm high-resolution Q75 chronology with the power transformation applied has a significant response at lag 1.

4. Discussion

The high-resolution aMXD has a stronger correlation with temperature across all frequencies, whereas the low-resolution aMXD has a sharp decline in its correlation with temperature when applying a low-pass filter (Figure 3b). We interpret these results as showing that the high-resolution aMXD reconstruction of past temperature is likely more accurate than the low-resolution, particularly for low-frequency climate variability. We hypothesize that high-resolution aMXD has stronger correlation with temperature due to the fine-scale precise measurements of the last rows of cells, which are the most sensitive to temperature and therefore record the strongest climate signals (Cuny & Rathgeber, 2016; Friend et al., 2022), whereas low-resolution aMXD performance is hindered because it aggregates cellular characteristics from a wider band. In narrow rings, and particularly in cases of narrow latewood width, low-resolution aMXD incorporates earlywood cell dimensions (96% of all the rings measured here have latewood width less than 80 μm). This inclusion of earlywood cells introduces additional non-climatic biological noise. Previous studies in temperate and boreal trees have found that earlywood cell characteristics do not have a single strong climate driver, and may be driven by photoperiod and hormonal controls (Castagneri et al., 2017; Cuny et al., 2014; Cuny & Rathgeber, 2016; Rossi et al., 2006).

A wider measurement band (lower resolution) also leads to a systematic reduction in aMXD values for the narrow rings compared to wide rings, resulting in an increased correlation between low-resolution aMXD and ring width (Figure S5 in Supporting Information S1; Björklund et al., 2019). It has been shown that ring-width data can

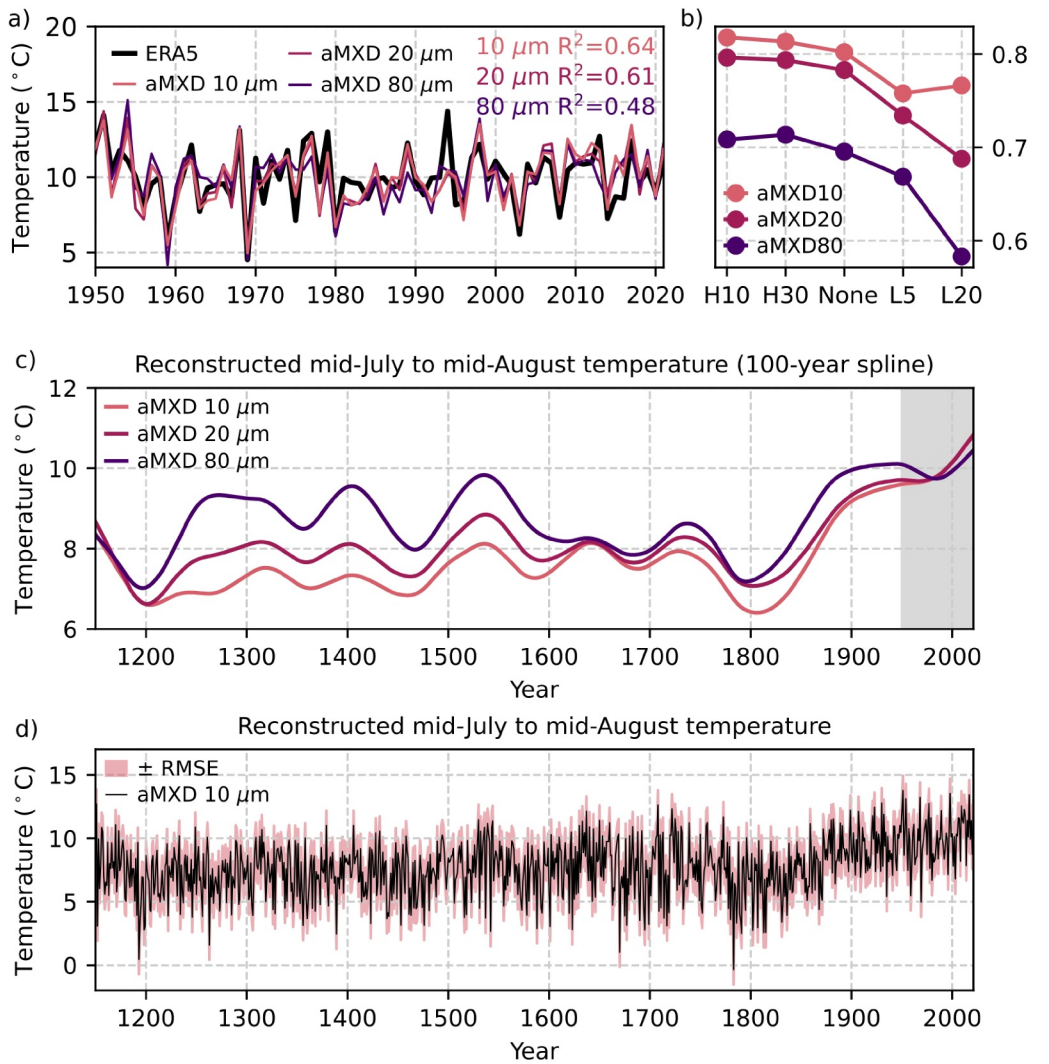

Figure 3. Mid-July to mid-August (195–223 DOY) temperature over the instrumental period, from ERA5 (black) and reconstructed using the aMXD chronologies at 10 (light red), 20 (magenta), and 80 μm (violet) resolution (a). Stability of 195–223 DOY temperature signal across frequencies for different aMXD resolutions. High-pass butterworth filter with 50% frequency response cut-off at 10 years (H10) and 30 years (H30). Low-pass butterworth filter with 50% frequency response cut-off at 5 years (L5) and 20 years (L20). Temperature and aMXD data were treated identically (b). Mid-July to mid-August (195–223 DOY) temperature full reconstruction from 1150 to 2021 CE using the aMXD chronologies at 10, 20, and 80 μm resolution smoothed with a 100-year cubic smoothing spline. The shaded gray box covers the instrumental period used for calibration (c). Reconstruction time series for the aMXD10 chronology without smoothing (d). Shaded envelope shows the ± RMSE.

exhibit amplified low-frequency signals and lagged effects due to growth processes responding to both climatic and non-climatic factors (Frank et al., 2007; Lücke et al., 2019). The low-resolution aMXD has more variability in the centennial and longer frequencies in the pre-industrial period spanning from 1150 to 1800 CE (Figure S6 in Supporting Information S1), showcasing the spectral biases known to be found in tree-ring width data (Esper et al., 2015; Franke et al., 2013). Additionally, ring width of high-latitude northwestern North American Picea is known to have very weak correlations with temperature at local scales (Briffa et al., 2002) that are unstable through time (Andreu-Hayles et al., 2011). The weaker correlation with temperature and red noise bias in low-resolution aMXD is therefore likely due to its similarity to and/or dependence on ring width (Figure S5 in Supporting Information S1).

The low-frequency behavior of the low-resolution aMXD, compared to that of the high-resolution aMXD, suggests that temperature reconstructions based on traditional MXD measurements–where the effective

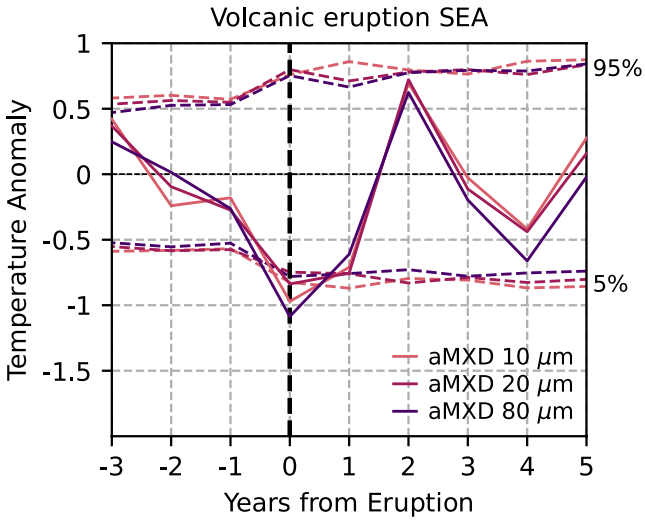

Figure 4. Superposed Epoch Analysis showing the composite mean temperature anomaly associated with the top 20 eruptions between 1150 and 1900 CE, determined by Northern Hemisphere stratospheric aerosol optical depth (Toohey & Sigl, 2017). The event years are 1171, 1182, 1230, 1257, 1286, 1329, 1345, 1453, 1458, 1477, 1585, 1600, 1640, 1695, 1729, 1783, 1809, 1815, 1831, and 1883. Reconstructions shown are the aMXD 10 (light red), 20 (magenta), and 80 μm (violet) resolution. Uncertainty bounds (5th and 95th percentile, dashed lines) are plotted in the same color as the composite responses for each reconstruction.

measurement resolution ranges from approximately 50 to 120 μm (Björklund et al., 2019)–may overestimate the low-frequency variability of the pre-industrial period. In contrast, climate models are thought to underestimate low-frequency variability of temperature compared to proxy data on the local scale, affecting detection and attribution studies (Collins et al., 2002; Ellerhoff & Rehfeld, 2021; Laepple et al., 2023; Lücke et al., 2019). Accounting for measurement resolution as a potential source of uncertainty in the low-frequency behavior of tree-ring based reconstructions could help reconcile proxy/model differences. In the case of the high-latitude Alaskan data presented here, this would lead to better detection, attribution, and understanding of Arctic amplification. Additionally, reducing errors in low-frequency variability by using high-resolution proxy data could improve equilibrium climate sensitivity estimates from the Common Era (Cropper et al., 2023).

The reconstructions presented here demonstrate how tree-ring measurement resolution significantly affects our understanding of pre-industrial temperature variability and its relationship to current warming trends. The high-resolution aMXD10 reconstruction (Figure 3d) shows a cooler pre-industrial period (1150–1850 CE) with a mean mid-July to mid-August temperature of 7.3°C, compared to 8.5°C for the lower resolution aMXD8 (Figure 3c) and 8.7°C for the original Firth River MXD data (Anchukaitis et al., 2013). Additionally, the high-resolution aMXD captures a larger industrial period warming trend (1850–2021 CE) than its lower resolution counterpart (Figure S7 in Supporting Information S1). Our high-resolution aMXD10 reconstruction also indicates a relatively cold late MCA. However, our record does not span the full length of the MCA climate period (950–1250 CE) and the inter-series agreement is low before 1200 CE (Figure S8 in Supporting Information S1) and therefore should be interpreted with caution. The original Firth River MXD from Anchukaitis et al. (2013) reconstructs a warmer late MCA compared to the aMXD across resolutions (Figure S9 in Supporting Information S1). These findings are consistent with those of Björklund et al. (2023), who found that MXD overestimates warming during the MCA compared to their QWA-based reconstructions. After the late MCA period, the temperature reconstructed based on aMXD10 slightly increases until the mid-18th century; the coldest temperatures in the Little Ice Age (LIA; 1450–1850 CE) do not emerge until the late 18th century (Figures 3c and 3d). The overall behavior of the high-resolution aMXD10 reconstruction suggests the Medieval epoch was cooler in northwestern North America than in previous reconstructions, which might be consistent with a lack of a globally coherent MCA or LIA (Goosse et al., 2012; Hughes & Diaz, 1994; Neukom et al., 2019).

The most significant difference between high-resolution and low-resolution aMXD reconstructions is in their low-frequency behavior, whereas the spectra for both low and high-resolution aMXD strongly overlap at the inter-annual frequencies (Figure S6 in Supporting Information S1). Our Firth River reconstruction shows eruption-year (Year 0) cooling in response to major volcanic eruptions (Figure 4). The magnitude of this cooling varies depending on chronology parameters, but the timing of the response remains consistent; only the 10 μm Q75 chronology SEA has statistically significant lag-1 cooling. Temperature reconstruction response to large volcanic eruptions and comparison to model simulations depends on multiple factors which can affect the final response magnitude and recovery behavior (Anchukaitis & Smerdon, 2022; Wang et al., 2023). In general ring-width based reconstructions have a muted and lagged volcanic cooling signal, whereas MXD-based reconstructions have an abrupt temperature decrease following eruptions and a protracted recovery, though not as severe as the lagged recovery in ring-width based reconstructions (D'Arrigo et al., 2013; Esper et al., 2015; Lücke et al., 2019; Schneider et al., 2015; Zhu et al., 2020). Therefore, despite its similarities to ring width, low-resolution aMXD still functions similarly to MXD in its response to large volcanic eruptions, exhibiting an abrupt temperature decrease followed by a quick recovery.

5. Conclusions

Our study shows that high-resolution aMXD provides a more accurate record of climate variability. The superior performance of high-resolution aMXD across multiple frequencies demonstrates that it offers a stronger calibration against instrumental data and better captures recent temperature trends. High-resolution cellular-scale measurements appear to reduce the influence of biological noise in chronologies and to enhance the representation of low-frequency variability, leading to better representation of temperature signals. These results collectively demonstrate the benefit of developing high-resolution wood anatomical data for the purposes of temperature reconstruction, particularly at the multi-centennial scale. Our study and other recent publications (e.g., Björklund et al., 2023; Seftigen et al., 2022) therefore show that QWA data provide novel high-resolution information that can affect the interpretation of low-frequency changes in past temperatures. Moreover, QWA data can improve temperature reconstructions from degraded relict wood, as cell-wall dimensions appear unaffected by abiotic decay compared to traditional density measurements (Klesse et al., 2025). QWA has the advantage of requiring fewer samples for robust chronology development (e.g., Björklund et al., 2020; Lopez-Saez et al., 2023; Seftigen et al., 2022), reducing the problem of declining sample depth in the earlier portions of reconstructions. QWA data also allow us to capture discrete, transient, intra-annual, and synoptic events (e.g., Edwards et al., 2021, 2022; Leland et al., 2025; Mayer et al., 2020; Piermattei et al., 2020). Thus the benefits of QWA analysis that arise from measurement resolution make the investment in this intensive method worthwhile for paleoclimatology across a range of timescales.

Conflict of Interest

The authors declare no conflicts of interest relevant to this study.

Data Availability Statement

The aMXD data generated as part of this study, and the code used to perform data analysis and to produce the manuscript's figures are available on Github https://github.com/JulieEdwardsPaleo/Firth and are archived in a Zenodo repository: Edwards (2025). The CRUST program is available at https://github.com/ClimaticResearchUnit/CRUST. ECMWF Reanalysis version 5 surface air temperature data is available from Hersbach et al. (2020), available at https://www.ecmwf.int/en/forecasts/dataset/ecmwf-reanalysis-v5.

Acknowledgments
This research was funded by Grants AGS-2102993 and ANS-2124889 from the US National Science Foundation. R.D.D. and L.A-H acknowledge NSF 2124885. L.A-H acknowledges Grant PID2021-126411OB-I00 funded by MICIU/AEI/10.13039/501100011033 and by "ERDF A way of making Europe." GvA was supported by the Swiss National Science Foundation SNSF (Grants 200021_182398, XELLCLIM and 200021L-227746, RECONSPHERE). We are grateful for fieldwork assistance from Max Torbenson and Inga Homfeld. Previous sampling and analysis of the Firth River chronology was supported by US NSF Grants 0211583, 0902051, and 1501834.

References

Anchukaitis, K. J., D'Arrigo, R. D., Andreu-Hayles, L., Frank, D., Verstege, A., Curtis, A., et al. (2013). Tree-ring-reconstructed summer temperatures from northwestern North America during the last nine centuries. *Journal of Climate*, *26*(10), 3001–3012. https://doi.org/10.1175/JCLI-D-11-00139.1

Anchukaitis, K. J., & Smerdon, J. E. (2022). Progress and uncertainties in global and hemispheric temperature reconstructions of the Common Era. *Quaternary Science Reviews*, *286*, 107537. https://doi.org/10.1016/j.quascirev.2022.107537

Anchukaitis, K. J., Wilson, R., Briffa, K. R., Büntgen, U., Cook, E. R., D'Arrigo, R., et al. (2017). Last millennium northern hemisphere summer temperatures from tree rings: Part II, spatially resolved reconstructions. *Quaternary Science Reviews*, *163*, 1–22. https://doi.org/10.1016/j.quascirev.2017.02.020

Andreu-Hayles, L., D'Arrigo, R., Anchukaitis, K. J., Beck, P. S., Frank, D., & Goetz, S. (2011). Varying boreal forest response to Arctic environmental change at the Firth River, Alaska. *Environmental Research Letters*, *6*(4), 045503. https://doi.org/10.1088/1748-9326/6/4/045503

Battipaglia, G., Frank, D., Büntgen, U., Dobrovolnỳ, P., Brázdil, R., Pfister, C., & Esper, J. (2010). Five centuries of Central European temperature extremes reconstructed from tree-ring density and documentary evidence. *Global and Planetary Change*, *72*(3), 182–191. https://doi.org/10.1016/j.gloplacha.2010.02.004

Björklund, J., Arx, G., Nievergelt, D., Wilson, R., den Bulcke, J. V., Günther, B., et al. (2019). Scientific merits and analytical challenges of tree-ring densitometry. *Reviews of Geophysics*, *57*(4), 1224–1264. https://doi.org/10.1029/2019rg000642

Björklund, J., Seftigen, K., Fonti, P., Nievergelt, D., & von Arx, G. (2020). Dendroclimatic potential of dendroanatomy in temperature-sensitive Pinus sylvestris. *Dendrochronologia*, *60*, 125673. https://doi.org/10.1016/j.dendro.2020.125673

Björklund, J., Seftigen, K., Stoffel, M., Fonti, M. V., Kottlow, S., Frank, D. C., et al. (2023). Fennoscandian tree-ring anatomy shows a warmer modern than medieval climate. *Nature*, *620*(7972), 97–103. https://doi.org/10.1038/s41586-023-06176-4

Bretherton, C. S., Widmann, M., Dymnikov, V. P., Wallace, J. M., & Bladé, I. (1999). The effective number of spatial degrees of freedom of a time-varying field. *Journal of Climate*, *12*(7), 1990–2009. https://doi.org/10.1175/1520-0442(1999)012<1990:tenosd>2.0.co;2

Briffa, K. R., Jones, P. D., Schweingruber, F. H., Karlén, W., & Shiyatov, S. G. (1996). Tree-ring variables as proxy-climate indicators: Problems with low-frequency signals. In *Climatic variations and forcing mechanisms of the last 2000 years* (pp. 9–41).

Briffa, K. R., & Melvin, T. M. (2011). A closer look at regional curve standardization of tree-ring records: Justification of the need, a warning of some pitfalls, and suggested improvements in its application. In M. K. Hughes, H. F. Diaz, & T. W. Swetnam (Eds.), *Dendroclimatology: Progress and prospects* (Vol. 11, pp. 113–146). Springer Verlag.

Briffa, K. R., Osborn, T. J., Schweingruber, F. H., Jones, P. D., Shiyatov, S. G., & Vaganov, E. A. (2002). Tree-ring width and density data around the northern Hemisphere: Part 1, local and regional climate signals. *The Holocene*, *12*(6), 737–757. https://doi.org/10.1191/0959683602hl587rp

Büntgen, U. (2022). Scrutinizing tree-ring parameters for Holocene climate reconstructions. *Wiley Interdisciplinary Reviews: Climate Change*, *13*(4), e778. https://doi.org/10.1002/wcc.778

Büntgen, U., Allen, K., Anchukaitis, K. J., Arseneault, D., Boucher, É., Bräuning, A., et al. (2021). The influence of decision-making in tree ring-based climate reconstructions. *Nature Communications*, *12*(1), 3411. https://doi.org/10.1038/s41467-021-23627-6

Campbell, R., McCarroll, D., Loader, N. J., Grudd, H., Robertson, I., & Jalkanen, R. (2007). Blue intensity in *Pinus sylvestris* tree-rings: Developing a new palaeoclimate proxy. *The Holocene*, *17*(6), 821–828. https://doi.org/10.1177/0959683607080523

Castagneri, D., Fonti, P., von Arx, G., & Carrer, M. (2017). How does climate influence xylem morphogenesis over the growing season? Insights from long-term intra-ring anatomy in *Picea abies*. *Annals of Botany*, *119*(6), 1011–1020. https://doi.org/10.1093/aob/mcw274

Christiansen, B., & Ljungqvist, F. C. (2017). Challenges and perspectives for large-scale temperature reconstructions of the past two millennia. *Reviews of Geophysics*, *55*(1), 40–96. https://doi.org/10.1002/2016rg000521

Collins, M., Osborn, T. J., Tett, S. F. B., Briffa, K. R., & Schweingruber, F. H. (2002). A comparison of the variability of a climate model with paleotemperature estimates from a network of tree-ring densities. *Journal of Climate*, *15*(13), 1497–1515. https://doi.org/10.1175/1520-0442(2002)015<1497:acotvo>2.0.co;2

Cook, E. R., Briffa, K., Shiyatov, S., & Mazepa, V. (1990). Estimation of the mean chronology. In *Methods of dendrochronology: Applications in the environmental sciences* (pp. 123–132). Kluwer Academic Publishers.

Cook, E. R., Briffa, K. R., Meko, D. M., Graybill, D. A., & Funkhouser, G. (1995). The segment length curse in long tree-ring chronology development for paleoclimatic studies. *The Holocene*, *5*(2), 229–237. https://doi.org/10.1177/095968369500500211

Cook, E. R., & Peters, K. (1997). Calculating unbiased tree-ring indices for the study of climatic and environmental change. *The Holocene*, *7*(3), 361–370. https://doi.org/10.1177/095968369700700314

Cropper, S., Thackeray, C., & Emile-Geay, J. (2023). Revisiting a constraint on equilibrium climate sensitivity from a last millennium perspective. *Geophysical Research Letters*, *50*(20), e2023GL104126. https://doi.org/10.1029/2023gl104126

Cuny, H. E., & Rathgeber, C. B. (2016). Xylogenesis: Coniferous trees of temperate forests are listening to the climate tale during the growing season but only remember the last words. *Plant Physiology*, *171*(1), 306–317. https://doi.org/10.1104/pp.16.00037

Cuny, H. E., Rathgeber, C. B. K., Frank, D., Fonti, P., & Fournier, M. (2014). Kinetics of tracheid development explain conifer tree-ring structure. *New Phytologist*, *203*(4), 1231–1241. https://doi.org/10.1111/nph.12871

D'Arrigo, R., Davi, N., Jacoby, G., Wilson, R., & Wiles, G. (2014). *Dendroclimatic studies: Tree growth and climate change in northern forests*. John Wiley & Sons.

D'Arrigo, R., Wilson, R., & Anchukaitis, K. J. (2013). Volcanic cooling signal in tree ring temperature records for the past millennium. *Journal of Geophysical Research: Atmospheres*, *118*(16), 9000–9010. https://doi.org/10.1002/jgrd.50692

Denne, M. (1989). Definition of latewood according to Mork (1928). *IAWA Journal*, *10*(1), 59–62. https://doi.org/10.1163/22941932-90001112

Edwards, J. (2025). Julieedwardspaleo/firth: Oct2025 (v1.0.0). *Zenodo*. https://doi.org/10.5281/zenodo.17363313

Edwards, J., Anchukaitis, K. J., Gunnarson, B. E., Pearson, C., Seftigen, K., von Arx, G., & Linderholm, H. W. (2022). The origin of tree-ring reconstructed summer cooling in northern Europe during the 18th century eruption of Laki. *Paleoceanography and Paleoclimatology*, *37*(2), e2021PA004386. https://doi.org/10.1029/2021pa004386

Edwards, J., Anchukaitis, K. J., Zambri, B., Andreu-Hayles, L., Oelkers, R., D'Arrigo, R., & von Arx, G. (2021). Intra-annual climate anomalies in northwestern North America following the 1783–1784 CE Laki eruption. *Journal of Geophysical Research: Atmospheres*, *126*(3), e2020JD033544. https://doi.org/10.1029/2020jd033544

Edwards, J., Tintor, W. L., Nolin, A. F., Woodhouse, C. A., von Arx, G., & Anchukaitis, K. J. (2025). Multiple elevation-dependent climate signals from quantitative wood anatomical measurements of Rocky Mountain bristlecone pine. *Journal of Geophysical Research: Biogeosciences*, *130*(1), e2024JG008307. https://doi.org/10.1029/2024jg008307

Ellerhoff, B., & Rehfeld, K. (2021). Probing the timescale dependency of local and global variations in surface air temperature from climate simulations and reconstructions of the last millennia. *Physical Review E*, *104*(6), 064136. https://doi.org/10.1103/physreve.104.064136

Esper, J., Frank, D. C., Timonen, M., Zorita, E., Wilson, R. J. S., Luterbacher, J., et al. (2012). Orbital forcing of tree-ring data. *Nature Climate Change*, *2*(12), 862–866. https://doi.org/10.1038/nclimate1589

Esper, J., Frank, D. C., & Wilson, R. J. (2004). Climate reconstructions: Low-frequency ambition and high-frequency ratification. *EOS, Transactions American Geophysical Union*, *85*(12), 113–120. https://doi.org/10.1029/2004eo120002

Esper, J., Krusic, P. J., Ljungqvist, F. C., Luterbacher, J., Carrer, M., Cook, E., et al. (2016). Ranking of tree-ring based temperature reconstructions of the past millennium. *Quaternary Science Reviews*, *145*, 134–151. https://doi.org/10.1016/j.quascirev.2016.05.009

Esper, J., Schneider, L., Smerdon, J. E., Schöne, B. R., & Büntgen, U. (2015). Signals and memory in tree-ring width and density data. *Dendrochronologia*, *35*, 62–70. https://doi.org/10.1016/j.dendro.2015.07.001

Fonti, M. V., von Arx, G., Harroue, M., Schneider, L., Nievergelt, D., Björklund, J., et al. (2025). A protocol for high-quality sectioning for tree-ring anatomy. *Frontiers in Plant Science*, *16*, 1505389. https://doi.org/10.3389/fpls.2025.1505389

Frank, D., Büntgen, U., Böhm, R., Maugeri, M., & Esper, J. (2007). Warmer early instrumental measurements versus colder reconstructed temperatures: Shooting at a moving target. *Quaternary Science Reviews*, *26*(25–28), 3298–3310. https://doi.org/10.1016/j.quascirev.2007.08.002

Franke, J., Frank, D., Raible, C. C., Esper, J., & Brönnimann, S. (2013). Spectral biases in tree-ring climate proxies. *Nature Climate Change*, *3*(4), 360–364. https://doi.org/10.1038/nclimate1816

Friend, A. D., Eckes-Shephard, A. H., & Tupker, Q. (2022). Wood structure explained by complex spatial source-sink interactions. *Nature Communications*, *13*(1), 7824. https://doi.org/10.1038/s41467-022-35451-7

Gärtner, H., & Schweingruber, F. (2013). *Microscopic preparation techniques for plant stem analysis* (Vol. 34). Kessel Publishing House.

Gershunov, A., Schneider, N., & Barnett, T. (2001). Low-frequency modulation of the ENSO-Indian monsoon rainfall relationship: Signal or noise? *Journal of Climate*, *14*(11), 2486–2492. https://doi.org/10.1175/1520-0442(2001)014<2486:lfmote>2.0.co;2

Goosse, H., Crespin, E., Dubinkina, S., Loutre, M.-F., Mann, M. E., Renssen, H., et al. (2012). The role of forcing and internal dynamics in explaining the "Medieval Climate Anomaly". *Climate Dynamics*, *39*(12), 2847–2866. https://doi.org/10.1007/s00382-012-1297-0

Hacke, U. G., Sperry, J. S., Pockman, W. T., Davis, S. D., & McCulloh, K. A. (2001). Trends in wood density and structure are linked to prevention of xylem implosion by negative pressure. *Oecologia*, *126*(4), 457–461. https://doi.org/10.1007/s004420100628

Hersbach, H., Bell, B., Berrisford, P., Hirahara, S., Horányi, A., Muñoz-Sabater, J., et al. (2020). The ERA5 global reanalysis. *Quarterly Journal of the Royal Meteorological Society*, *146*(730), 1999–2049. https://doi.org/10.1002/qj.3803

Homfeld, I. K., Büntgen, U., Reinig, F., Torbenson, M. C., & Esper, J. (2024). Application of RCS and signal-free RCS to tree-ring width and maximum latewood density data. *Dendrochronologia*, *85*, 126205. https://doi.org/10.1016/j.dendro.2024.126205

Hughes, M. K., & Diaz, H. F. (1994). Was there a 'Medieval Warm Period', and if so, where and when? *Climatic Change*, *26*(2), 109–142. https://doi.org/10.1007/bf01092410

Jevšenak, J. (2019). Daily climate data reveal stronger climate-growth relationships for an extended European tree-ring network. *Quaternary Science Reviews*, *221*, 105868. https://doi.org/10.1016/j.quascirev.2019.105868

Jones, P. D., & Mann, M. E. (2004). Climate over past millennia. *Reviews of Geophysics*, *42*(2). https://doi.org/10.1029/2003rg000143

Katzenmaier, M., Garnot, V. S. F., Björklund, J., Schneider, L., Wegner, J. D., & von Arx, G. (2023). Towards ROXAS AI: Deep learning for faster and more accurate conifer cell analysis. *Dendrochronologia*, *81*, 126126. https://doi.org/10.1016/j.dendro.2023.126126

Klesse, S., Björklund, J., Fonti, M. V., Nievergelt, D., von Arx, G., Hantemirov, R. M., et al. (2025). Tree-ring anatomy improves the reliability of temperature reconstructions using relict wood. *Geophysical Research Letters*, *52*(8), e2024GL113310. https://doi.org/10.1029/2024gl113310

Laepple, T., Ziegler, E., Weitzel, N., Hébert, R., Ellerhoff, B., Schoch, P., et al. (2023). Regional but not global temperature variability underestimated by climate models at supradecadal timescales. *Nature Geoscience*, *16*(11), 958–966. https://doi.org/10.1038/s41561-023-01299-9

Leland, C., Davi, N., D'Arrigo, R., Andreu-Hayles, L., Pacheco-Solana, A., Edwards, J., et al. (2025). Tree-ring evidence of the elusive 1959 summer cold event in northwestern North America. *Arctic Antarctic and Alpine Research*, *57*(1), 2445945. https://doi.org/10.1080/15230430.2024.2445945

Lopez-Saez, J., Corona, C., Von Arx, G., Fonti, P., Slamova, L., & Stoffel, M. (2023). Tree-ring anatomy of Pinus cembra trees opens new avenues for climate reconstructions in the European Alps. *Science of the Total Environment*, *855*, 158605. https://doi.org/10.1016/j.scitotenv.2022.158605

Lücke, L. J., Hegerl, G. C., Schurer, A. P., & Wilson, R. (2019). Effects of memory biases on variability of temperature reconstructions. *Journal of Climate*, *32*(24), 8713–8731. https://doi.org/10.1175/jcli-d-19-0184.1

Lücke, L. J., Schurer, A. P., Wilson, R., & Hegerl, G. C. (2021). Orbital forcing strongly influences seasonal temperature trends during the last millennium. *Geophysical Research Letters*, *48*(4), e2020GL088776. https://doi.org/10.1029/2020gl088776

Mann, M. E., & Jones, P. D. (2003). Global surface temperatures over the past two millennia. *Geophysical Research Letters*, *30*(15). https://doi.org/10.1029/2003gl017814

Masson-Delmotte, V., Zhai, P., Pirani, A., Connors, S. L., Péan, C., Berger, S., et al. (2021). *Climate Change 2021: The physical science basis. Contribution of working group I to the sixth assessment report of the intergovernmental panel on climate change*. Cambridge University Press.

Mayer, K., Grabner, M., Rosner, S., Felhofer, M., & Gierlinger, N. (2020). A synoptic view on intra-annual density fluctuations in Abies alba. *Dendrochronologia*, *64*, 125781. https://doi.org/10.1016/j.dendro.2020.125781

McCarroll, D., Pettigrew, E., Luckman, A., Guibal, F., & Edouard, J.-L. (2002). Blue reflectance provides a surrogate for latewood density of high-latitude pine tree rings. *Arctic Antarctic and Alpine Research*, *34*(4), 450–453. https://doi.org/10.1080/15230430.2002.12003516

McCarroll, D., Young, G. H., & Loader, N. J. (2015). Measuring the skill of variance-scaled climate reconstructions and a test for the capture of extremes. *The Holocene*, *25*(4), 618–626. https://doi.org/10.1177/0959683614565956

Meko, D. M., & Woodhouse, C. A. (2011). Application of streamflow reconstruction to water resources management. In *Dendroclimatology: Progress and prospects* (pp. 231–261). Springer. https://doi.org/10.1007/978-1-4020-5725-0_8

Melvin, T. M., & Briffa, K. (2008). A 'signal-free' approach to dendroclimatic standardisation. *Dendrochronologia*, *26*(2), 71–86. https://doi.org/10.1016/j.dendro.2007.12.001

Melvin, T. M., & Briffa, K. R. (2014a). CRUST: Software for the implementation of regional chronology standardisation: Part 1. Signal-free RCS. *Dendrochronologia*, *32*(1), 7–20. https://doi.org/10.1016/j.dendro.2013.06.002

Melvin, T. M., & Briffa, K. R. (2014b). CRUST: Software for the implementation of regional chronology standardisation: Part 2. Further RCS options and recommendations. *Dendrochronologia*, *32*(4), 343–356. https://doi.org/10.1016/j.dendro.2014.07.008

Melvin, T. M., Briffa, K. R., Nicolussi, K., & Grabner, M. (2007). Time-varying-response smoothing. *Dendrochronologia*, *25*(1), 65–69. https://doi.org/10.1016/j.dendro.2007.01.004

Mork, E. (1928). Die qualität dês fichtenholzes unter besonderer rucksichtnahme auf Schleif-und Papierholz. *Papier-fabrikant*, *26*, 741–747.

Neukom, R., Steiger, N., Gómez-Navarro, J. J., Wang, J., & Werner, J. P. (2019). No evidence for globally coherent warm and cold periods over the preindustrial Common Era. *Nature*, *571*(7766), 550–554. https://doi.org/10.1038/s41586-019-1401-2

Ols, C., Klesse, S., Girardin, M. P., Evans, M. E., DeRose, R. J., & Trouet, V. (2023). Detrending climate data prior to climate–growth analyses in dendroecology: A common best practice? *Dendrochronologia*, *79*, 126094. https://doi.org/10.1016/j.dendro.2023.126094

PAGES 2k Consortium. (2019). Consistent multidecadal variability in global temperature reconstructions and simulations over the Common Era. *Nature Geoscience*, *12*(8), 643–649. https://doi.org/10.1038/s41561-019-0400-0

Piermattei, A., Crivellaro, A., Krusic, P. J., Esper, J., Vítek, P., Oppenheimer, C., et al. (2020). A millennium-long 'Blue Ring' chronology from the Spanish Pyrenees reveals severe ephemeral summer cooling after volcanic eruptions. *Environmental Research Letters*, *15*(12), 124016. https://doi.org/10.1088/1748-9326/abc120

Prendin, A. L., Petit, G., Carrer, M., Fonti, P., Björklund, J., & von Arx, G. (2017). New research perspectives from a novel approach to quantify tracheid wall thickness. *Tree Physiology*, *37*(7), 976–983. https://doi.org/10.1093/treephys/tpx037

Rossi, S., Deslauriers, A., Anfodillo, T., Morin, H., Saracino, A., Motta, R., & Borghetti, M. (2006). Conifers in cold environments synchronize maximum growth rate of tree-ring formation with day length. *New Phytologist*, *170*(2), 301–310. https://doi.org/10.1111/j.1469-8137.2006.01660.x

Rydval, M., Björklund, J., von Arx, G., Begović, K., Lexa, M., Nogueira, J., et al. (2024). Ultra-high-resolution reflected-light imaging for dendrochronology. *Dendrochronologia*, *83*, 126160. https://doi.org/10.1016/j.dendro.2023.126160

Rydval, M., Larsson, L.-Å., McGlynn, L., Gunnarson, B. E., Loader, N. J., Young, G. H., & Wilson, R. (2014). Blue intensity for dendroclimatology: Should we have the blues? Experiments from Scotland. *Dendrochronologia*, *32*(3), 191–204. https://doi.org/10.1016/j.dendro.2014.04.003

Schneider, L., Smerdon, J. E., Büntgen, U., Wilson, R. J. S., Myglan, V. S., Kirdyanov, A. V., & Esper, J. (2015). Revising midlatitude summer temperatures back to A.D. 600 based on a wood density network. *Geophysical Research Letters*, *42*(11), 4556–4562. https://doi.org/10.1002/2015gl063956

Seftigen, K., Fonti, M. V., Luckman, B., Rydval, M., Stridbeck, P., von Arx, G., et al. (2022). Prospects for dendroanatomy in paleoclimatology–a case study on *Picea engelmannii* from the Canadian Rockies. *Climate of the Past*, *18*(5), 1151–1168. https://doi.org/10.5194/cp-18-1151-2022

Stoffel, M., Khodri, M., Corona, C., Guillet, S., Poulain, V., Bekki, S., et al. (2015). Estimates of volcanic-induced cooling in the Northern Hemisphere over the past 1,500 years. *Nature Geoscience*, *8*(10), 784–788. https://doi.org/10.1038/ngeo2526

Stokes, M., & Smiley, T. (1968). *An introduction to tree-ring dating*. University of Chicago Press.

Tierney, J. E., Poulsen, C. J., Montañez, I. P., Bhattacharya, T., Feng, R., Ford, H. L., et al. (2020). Past climates inform our future. *Science*, *370*(6517), eaay3701. https://doi.org/10.1126/science.aay3701

Toohey, M., & Sigl, M. (2017). Volcanic stratospheric sulfur injections and aerosol optical depth from 500 BCE to 1900 CE. *Earth System Science Data*, *9*(2), 809–831. https://doi.org/10.5194/essd-9-809-2017

Vaganov, E. A., Hughes, M. K., & Shashkin, A. V. (2006). *Growth dynamics of conifer tree rings: images of past and future environments* (Vol. 183). Springer Science & Business Media.

von Arx, G., & Carrer, M. (2014). ROXAS–A new tool to build centuries-long tracheid-lumen chronologies in conifers. *Dendrochronologia*, *32*(3), 290–293. https://doi.org/10.1016/j.dendro.2013.12.001

von Arx, G., Crivellaro, A., Prendin, A. L., Čufar, K., & Carrer, M. (2016). Quantitative wood anatomy—practical guidelines. *Frontiers in Plant Science*, *7*, 781. https://doi.org/10.3389/fpls.2016.00781

Wang, F., Arseneault, D., Boucher, É., Gennaretti, F., Lapointe, F., Yu, S., & Francus, P. (2023). Volcanic imprints in last-millennium land summer temperatures in the circum–North Atlantic area. *Journal of Climate*, *36*(17), 5923–5939. https://doi.org/10.1175/jcli-d-23-0107.1

Wilson, R., Anchukaitis, K. J., Briffa, K. R., Büntgen, U., Cook, E., D'Arrigo, R., et al. (2016). Last millennium northern hemisphere summer temperatures from tree rings: Part I: The long term context. *Quaternary Science Reviews*, *134*, 1–18. https://doi.org/10.1016/j.quascirev.2015.12.005

Zhu, F., Emile-Geay, J., Hakim, G. J., King, J., & Anchukaitis, K. J. (2020). Resolving the differences in the simulated and reconstructed temperature response to volcanism. *Geophysical Research Letters*, *47*(8), e2019GL086908. https://doi.org/10.1029/2019gl086908

References From the Supporting Information

Bunn, A. G. (2008). A dendrochronology program library in R (dplR). *Dendrochronologia*, *26*(2), 115–124. https://doi.org/10.1016/j.dendro.2008.01.002

Kruskal, W. H., & Wallis, W. A. (1952). Use of ranks in one-criterion variance analysis. *Journal of the American Statistical Association*, *47*(260), 586. https://doi.org/10.2307/2280779

Saltelli, A., Ratto, M., Andres, T., Campolongo, F., Cariboni, J., Gatelli, D., et al. (2008). *Global sensitivity analysis: The primer*. John Wiley & Sons.